Tectonophysics 578 (2012) 98–106

Contents lists available at SciVerse ScienceDirect

Tectonophysics

journal homepage: www.elsevier.com/locate/tecto

Vertical crustal motion of active plate convergence in Taiwan derived from tide gauge, altimetry, and GPS data

Emmy T.Y. Chang [a,*], Benjamin F. Chao [b,c], Chieh-Chung Chiang [a], Cheinway Hwang [d]

[a] Institute of Oceanography, National Taiwan University, Taipei, Taiwan
[b] Institute of Earth Sciences, Academia Sinica, Taipei, Taiwan
[c] College of Earth Sciences, National Central University, Chungli, Taiwan
[d] Dept. of Civil Engineering, National Chiao Tung University, Hsinchu, Taiwan

ARTICLE INFO

Article history:
Received 9 October 2010
Received in revised form 16 September 2011
Accepted 3 October 2011
Available online 12 October 2011

Keywords:
Tide gauge
Altimeter
GPS
Uplift
Subsidence
Convergence

ABSTRACT

Located at the converging junction between the Eurasian and Philippine Sea plates, the island of Taiwan is subject to an active lithospheric deformation as well as seismicity. Taking the difference between the satellite altimetry data (ALT) that give the absolute sea level variation and the tide gauge data (TG) that record the relative sea level variation, we obtain the absolute vertical crustal motion of the tide gauge sites. We use 20 TG stations along the west and east coasts of Taiwan along with the ALT measurements from the TOPEX/Poseidon–Jason satellites in the nearby waters. The ALT–TG results are compared with vertical GPS measurements in discussing vertical motion. We find a general subsidence of the entire Taiwan coast during the past two decades. The west coast sees no prominent vertical motion but with a severe local subsidence due to the over-withdrawal of groundwater. On the east coast, the ALT–TG results in the northern section demonstrate a northward dipping motion. The elastic thickness of the neighboring oceanic lithosphere modeled as an elastic plate with the flexure of the subducting plate shows that the adjacent Philippine Sea plate should be an old, thick oceanic plate, which could drag the slab into the mantle as manifested in a gentle northward subsidence in the northeast Taiwan. In the southern section of the east coast, the ALT–TG results reveal a segmented or undulating pattern in the vertical-motion rates. Judging from the different behaviors between the co-seismic and interseismic vertical motions marked by the major earthquakes during the studied period, we postulate a temporal saw-tooth scenario for the deformation in phases. It demonstrates the opposite motions under different mechanisms in the frontal sections of the subduction zone, which can be understood with lateral collision and slab dragging subject to varied temporal and spatial dependences.

1. Introduction

The crustal deformation has been measured by, among other geodetic means, the Global Positioning System (GPS). Since the 1990s GPS measurements have demonstrated that the present-day horizontal crustal motions conform largely to that predicted by plate tectonics based on geological evidences on million-year timescales. The discrepancies between the modern geodetic measurements and geological evidences are then source observation for refinement of the regional plate-motion models. Many such studies have been conducted to elucidate the Taiwan tectonics (e.g. Angelier et al., 2009; Chang et al., 2003; Rau et al., 2008; Wu et al., 2009; Yu and Kuo, 2001; Yu et al., 1997). On the other hand, for the vertical component of the crustal deformation, while gravimeters and other traditional geodetic sensors are routinely used to record the non-tectonic vertical motion due to tides, atmospheric and oceanic mass loadings, and regional post-glacial rebound, the tectonics-related or orogenic vertical motions have received comparatively less attention. One reason is the generally small magnitude of such vertical deformations during relatively short timespans of observation, compounded by the well-known fact that GPS data have much larger errors in the vertical than the horizontal components (e.g. Dixon, 1991; Hager et al., 1991).

Spanning 400 km N–S and lying on the western boundary of the Pacific–Eurasian plate convergence zone, the island of Taiwan is characterized by a double subduction system along two offshore trenches (Fig. 1), whose corresponding Wadati–Benioff zones are clearly delineated by the great number of subduction earthquakes recorded over the past several decades (Tsai, 1986). On the east, the Philippine Sea plate subducts under the Eurasian plate extending under northern Taiwan, which simultaneously upducts upon the Eurasian plate along the N–S trending Longitudinal Valley (LV) in eastern Taiwan, forming the E–W trending Ryukyu Trench along the latitude around 23.5°N. The LV is the suture zone between the Eurasian continent on the west and the Philippine Sea plate on the east. The Coastal

* Corresponding author at: Institute of Oceanography, National Taiwan University, No.1, Sec. 4, Roosevelt Rd. Taipei, Taiwan 106. Tel.: +886 2 3366 1629; fax: +886 2 2392 5294.
E-mail address: etychang@ntu.edu.tw (E.T.Y. Chang).

0040-1951/$ – see front matter © 2011 Elsevier B.V. All rights reserved.
doi:10.1016/j.tecto.2011.10.002

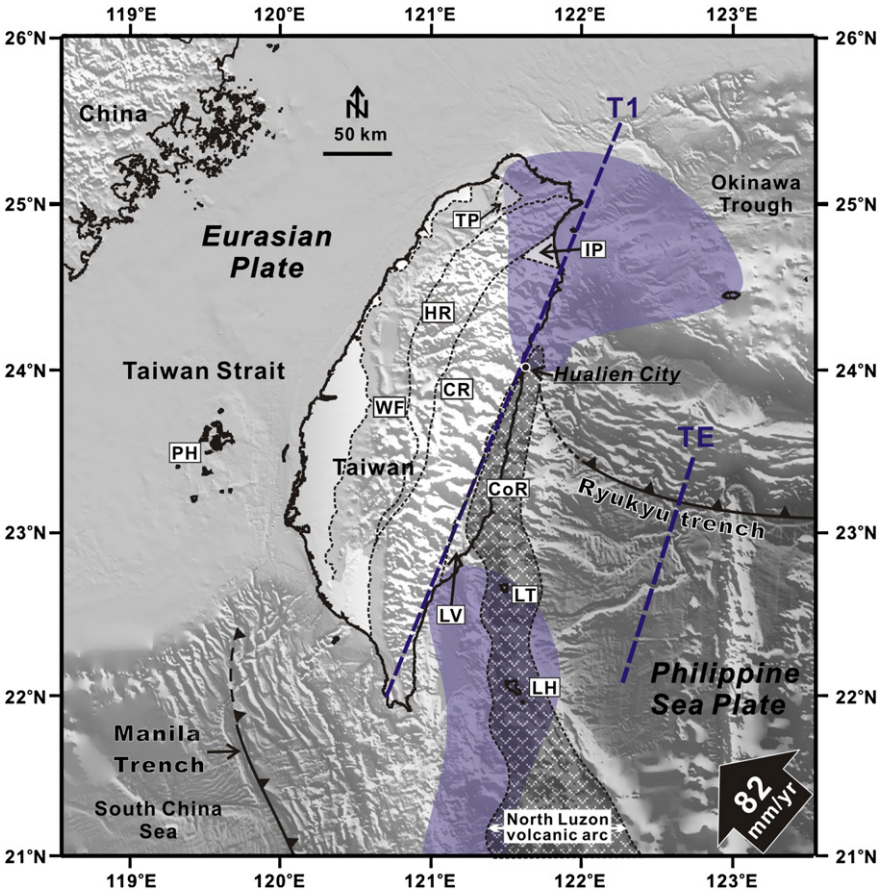

Fig. 1. Tectonic setting of Taiwan controlled by the two subduction systems at the Ryukyu and Manila trenches: The large black arrow at the lower-right gives the motion of the Philippine Sea plate relative to the Eurasian plate; the blue shadows show the surface projection of the two Wadati–Benioff zones identified from the seismicity of 50–150 km depth. Blue dashed lines (T1 and TE) indicate the profiles discussed in the text. (CoR: Coastal Range; CR: Central Range; HR: Hsuëshan Range; IP: Ilan Plain; LH: Lanyu islet; LT: Lutao islet; LV: Longitudinal Valley; PH: Penghu islet; TP: Taipei basin; WF: western foothill.)

Range east of LV has been considered to be part of the Philippine Sea plate (Ernst, 1977; Hsu, 1956), corroborated by its distinct surface motion (Yu et al., 1997). On the south, the subduction system of Taiwan is where the Eurasian plate subducts towards the east beneath the Philippine Sea plate, forming the N–S trending Manila Trench (Fig. 1). The vigorous orogeny between these two oblique subduction systems thus generates a great complexity in surface deformation of the Taiwan island.

In this study, we adopt two types of measurements that are sensitive to the vertical crustal deformation, even though not originally designed to do so — namely the tide gauge and the satellite ocean altimeter. A tide gauge records the coastal sea surface height (SSH) in a continuous fashion in time but relative to the tide gauge location fixed to the ground, while the ocean altimetry measures the "absolute" SSH in the geocentric terrestrial reference frame. Their difference, that is, the altimeter-determined SSH minus the tide gauge-determined SSH, thus signifies the crustal vertical deformation of the tide gauge location in an absolute sense (Cazenave et al., 1999; Mazzotti et al., 2008; Nerem and Mitchum, 2002). Such approach has successfully resolved recent vertical crustal motion of, for example, post-glacial isostatic rebound (Kuo et al., 2004) and the subsidence related to lithospheric plate subduction (García et al., 2007).

Thus, making use of the satellite ocean altimetry data with the long-term recordings from tide gauges around the island residing upon both the Philippine Sea and the Eurasian plates, we shall determine the vertical motion in the Taiwan coastal region. When compared against the independent, continuous GPS vertical measurements that are neighboring to the tide gauge, these results elucidate the complexity of the vertical deformation of Taiwan coasts and its geophysical mechanisms in the context of the plate convergence.

2. Data and analysis

The ocean radar altimetry data (ALT for short) used in this study are obtained from the satellite missions of TOPEX/Poseidon and its follow-on Jason-1, available from the DEOS/RADS data center (Delft Institute for Earth-Oriented Space research/Radar Altimeter Database System, also see http://rads.tudelft.nl/rads/). Satellite altimetry determines the distance from the satellite to the nadir surface by measuring the satellite-to-surface round-trip time of flight of a radar pulse. Knowing the satellite orbit (by ground or GPS tracking), one obtains SSH with respect to the reference ellipsoid for the given location at the given moment.

TOPEX/Poseidon was launched in 1992 into a 10-day repeat orbit of 66° inclination. The mission was followed by Jason-1 since 2001 (e.g. Schrama et al., 2000). The continuous ALT time series we use spans 16 years of 1992–2008 at 10-day intervals. Fig. 2 shows the TOPEX/Poseidon–Jason-1 altimetry 10-day repeat-orbit groundtracks near Taiwan (Passes # 051, 127, 164, and 240). Considering the regional variations of sea-level trend in the offshore area (Cazenave and Nerem, 2004; Church et al., 2004), five zones close to our tide gauge stations are selected in this study, indicated as A to E. Here the ALT time series is compiled from the sequence of spatially averaged SSH in the selected zone during each given satellite transect (zone B has two transects) (Figs. 2 and 3a). As is generally the case,

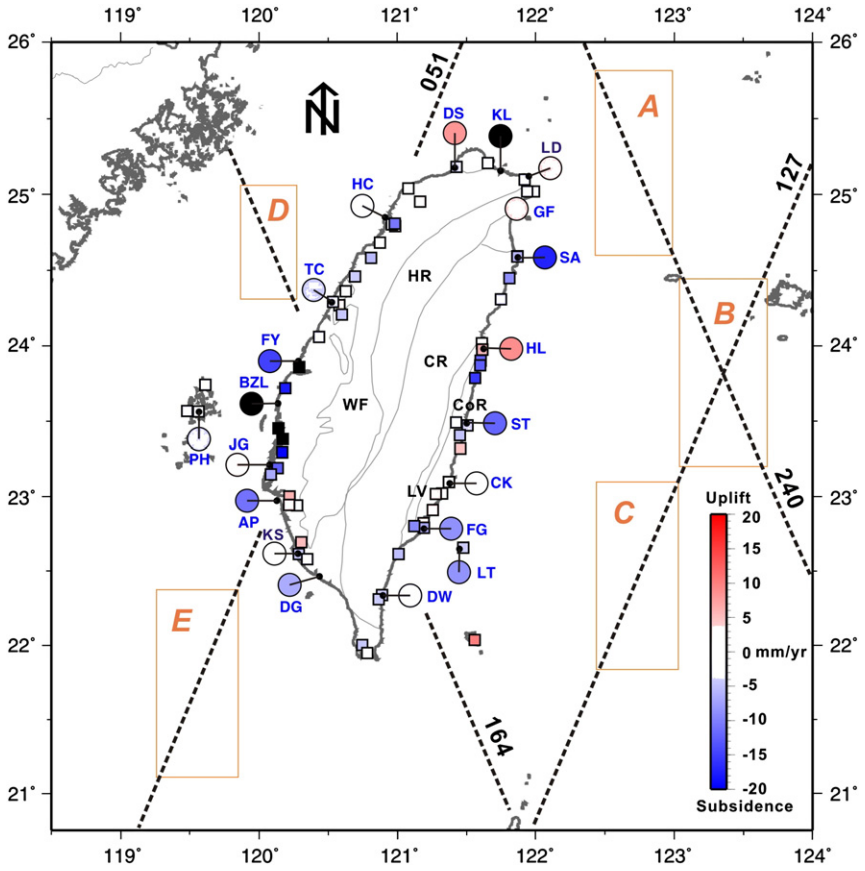

Fig. 2. Map view of the ALT–TG estimates (circles) as well as the GPS measurements (squares) of the vertical crustal motion, magnitude expressed in color. Black spots indicate the locations of the TG stations. TOPEX/Poseidon–Jason-1 (for ALT) ground tracks and the five selected zones (A–E) are shown. The GPS measurements affected by co-seismic motions are not presented.

the data too close to the coastlines are excluded because of the instrumental land contamination (e.g. Hwang et al., 2006; Vignudelli et al., 2005). Standard corrections have been made with the ALT RADS database including geophysical corrections (dry and wet troposphere and ionosphere), sea state bias, and various tidal effects. The TOPEX/Poseidon altimetry has achieved a general accuracy at 2–3 cm level, and Jason-1 approaches the 1 cm accuracy (Luthcke et al., 2003; Naeije et al., 2002; Schrama et al., 2000).

The tide gauge (TG) time series that we use are hourly records sustained by the Central Weather Bureau of Taiwan. There are 20 TG stations chosen along the coast of Taiwan and two off-shore islets (Stations LT and PH, see Fig. 2). Only well-maintained stations whose records show steady behavior are used, and we avoid records or record sections containing erratic or discontinuous motions, which are likely the result of equipment maintenance or generated by seismic activities (see examples of TG time series in Fig. 3(b)). We further remove large spurious transients caused by typhoons or other short-term meteorological effects as "outliers" with respect to the 2.5-standard deviation. The distances between the TG stations and the corresponding ALT zones range from 35 to 150 km; the long-term sea-level variability on at least decadal time scales is presumably insensitive to this spatial separation.

We thus model the time series of either ALT (t) or TG (t) as:

$$a_0 + a_1 t + \sum_i^n [A_i \sin(\omega_i t) + B_i \cos(\omega_i t)] + residual \quad (1)$$

where a_0, a_1, A_i, and B_i, are the coefficients to be estimated by least-squares fitting. The bracket in Eq.(1) represents the major tidal and seasonal terms with their known periods, including semi-diurnal tides (M_2, S_2, N_2, K_2, L_2, T_2, and $2N_2$), diurnal tides (K_1, O_1, P_1, and Q_1), the long-period tides (Msm, Mm, MSf, and Mf), and the annual and semi-annual terms (same as the Sa, Ssa long-period tides). These harmonic terms are then removed by subtraction as they are of no interest in this study. The coefficient a_1 represents the optimal estimate of the temporal rate, or linear trend, of the vertical motion, which is the parameter of interest here. The difference between the linear trends of ALT and TG should be able to give unequivocal information about the long-term vertical ground motion of the TG site itself — a positive value of the linear slope of the time series means the TG site is uplifting, and a negative value subsiding. Formal errors of the least-squares regression are evaluated by the general error propagation considering the standard deviation of recorded SSH and the data length used for regression (Taylor, 1997). The statistical uncertainty of the ALT–TG trend is determined from the variance-sum of the regression uncertainties of each ALT–TG pair, assuming non-correlation between the two.

We compare our ALT–TG results with the vertical motion independently measured by the continuous GPS stations along the coast of Taiwan. Here the GPS measurements are reported with respect to the International Terrestrial Reference Frame, the same reference for our ALT–TG values. The GPS time series are daily averaged values processed and compiled by the Data Center of the Taiwan Earthquake research Center (TECDC) (Hugentobler et al., 2001; Kuo, 2008; Yu et al., 1997) (for more information see TECDC website, http://tecdc.earth.sinica.edu.tw/, and the GPS service website: http://gps.earth.sinica.edu.tw/). The uncertainties of the GPS measurements are generally in the range of 0.2–0.6 mm/yr, depending partly on the time span of the given stations many of which were installed within the last decade.

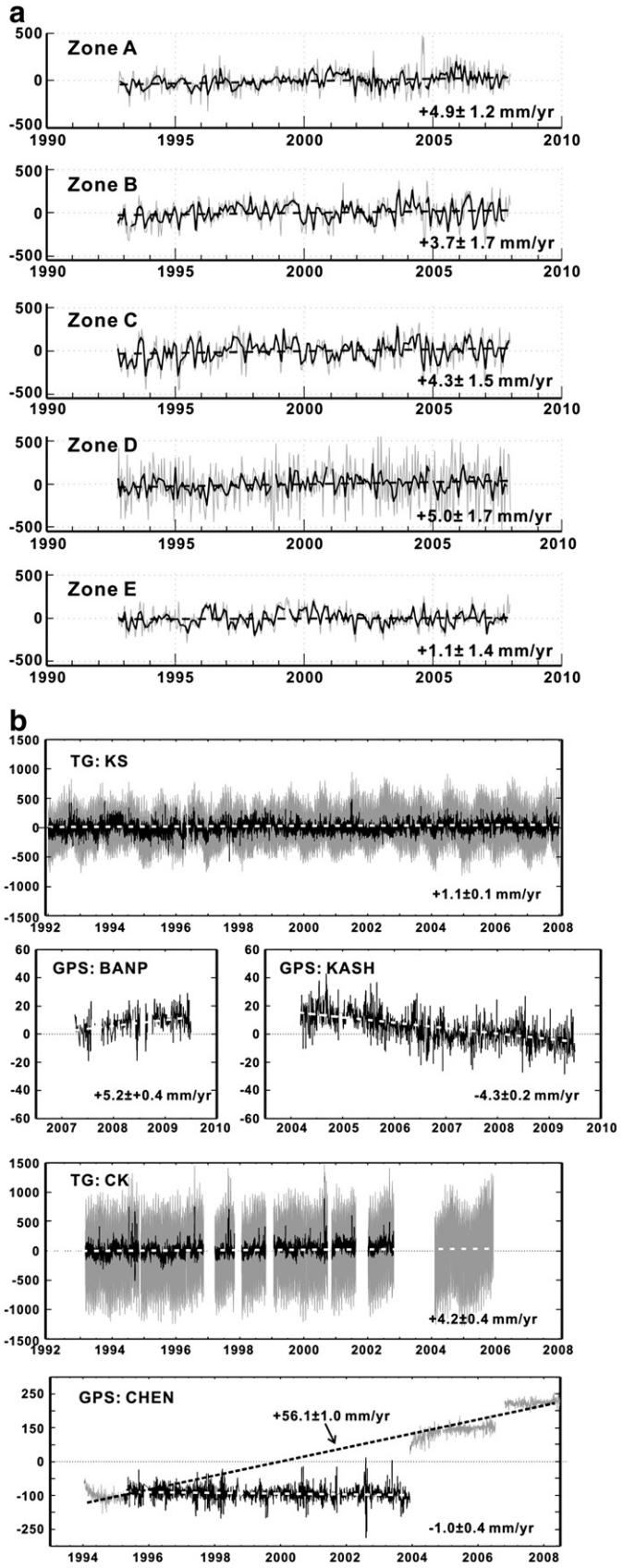

Fig. 3. (a) Time series from the five ALT data zones as a function of calendar year. Thin gray lines are the raw ALT series; black lines the monthly mean series. Thick dashed lines show the linear uplift trends estimated by least-squares regression. (b) Two TG time series at KS and CK, and their neighboring GPS observations. Thin gray lines are the raw TG time series; black lines the detided section used to determine the vertical rate. Thick dashed lines show the linear LS trends. Units are in mm.

3. Results

Fig. 3(a) presents the monthly-averaged ALT time series (which have been removed of the high-frequency constituents as above) of the five selected zones. Undulating monthly at about 200 or 250 mm, the absolute sea level around Taiwan appears to rise at the rate of 4.0–5.0 mm/yr, or twice the rate of the global sea-level rise (Tseng et al., 2009), except for Zone E located at the northern margin of the South China Sea which is at a much slower but uncertain rate of 1.1 ± 1.4 mm/yr.

Fig. 3(b) demonstrates two TG time series and their nearby GPS observations selected for a parallel comparison of vertical motions along the coast of Taiwan. Even though the magnitudes of the tidal constituents vary considerably at different locations around Taiwan, the detided residual TG time series reveal a minor undulation of less than 100 mm. Note that in a relatively short time span the GPS observations sometimes show opposite sense in the vertical motion from the neighboring stations, for example the stations BANP versus KASH (see Fig. 3(b)). Table 1 lists all the ALT–TG values for the vertical rate at the TG locations (see Fig. 2), and the corresponding nearby GPS measurements for comparison. The uncertainties in ALT–TG values are apparently much larger than those in GPS and seem to stem mainly from the relatively sparse sampling in the ALT series. Note that in general the ALT–TG results are derived from the data series longer than ten years, whereas the GPS are considerably shorter in time span. We therefore find it difficult and undesirable to estimate the ALT–TG rates from the difference time series of the two. For the cases where this is possible, our trial results show little difference between the two schemes.

Our comparison results are further summarized in Figs. 2 and 4. In Fig. 2, the vertical motion magnitude is indicated in shade of color with red meaning uplift (positive values) and blue subsidence (negative values). It is evident that, despite the difference in time spans adopted, the ALT–TG and GPS vertical motion measurements are in general agreement with each other, except for sites in the northern end of Taiwan around KL, and JG and AP just south of the station BZL in the western middle Taiwan (groundwater over-withdrawal region, see below). It is interesting to note that BZL and KL are also where the largest subsidences are seen (the colored shade in Fig. 2 is made to saturate, at ± 20 mm/yr, for subsidence at these stations).

It is evident that the vertical motions determined from both ALT–TG and GPS portray a general subsidence around most of the Taiwan coasts. ALT–TG and GPS results give predominantly negative values: the (unweighted) average ALT–TG rate is about -7.0 mm/yr and that of GPS -4.0 mm/yr, respectively. If we exclude the large (non-tectonic) subsidence around BZL, the dominant subsidence motion is somewhat reduced to about -4.5 mm/yr and -2.6 mm/yr, respectively. On the other hand, in a consistent manner both ALT–TG and GPS values show considerable spatial variability, sometimes quite locally.

4. Discussions

An apparent general subsidence found around the island coast confronts the notion that Taiwan as an island owes its very existence to the upward motion associated with a vigorous orogeny (e.g. Dadson et al., 2003; Ho, 1986). Furthermore, corroborating the subsiding motion detected at some local spots (e.g. Chang et al., 2004; Teng, 1996) and the strongly lateral motions reported in recent GPS observation (e.g. Angelier et al., 2009; Chiu et al., 2008), our complex spatial pattern of the vertical motion indicates local and varied responses to tectonic forcing, and would defy simplistic crustal deformation model of Taiwan. We shall discuss them in more detail below.

Table 1
Vertical motion rates obtained in this study. Positive values represent uplift, negative values subsidence.

(a) Vertical motion rate determined from ALT–TG

ALT[1]		TG[2]					ALT–TG
Zone	LS trend (mm/yr)	station			Data period (yr)	LS trend (mm/yr)	Vertical rate (mm/yr)
		Name	Long. (°E)	Lat.(°N)			
A	+4.9 ± 1.2	KL	121.744	25.157	1992–2002	+26.7 ± 0.5	−21.8 ± 1.3
		LD	121.950	25.120	2004–2007	+1.5 ± 1.6	+3.4 ± 2.0
		GF	121.862	24.907	1998–2007	+1.3 ± 0.3	+3.6 ± 1.2
		SA	121.869	24.586	1992–2005	+22.1 ± 3.1	−17.2 ± 3.3
B	+3.7 ± 1.7	HL	121.623	23.980	1997–2002	−5.2 ± 0.2	+8.9 ± 1.7
		ST	121.500	23.486	2001–2007	+15.8 ± 1.1	−12.1 ± 2.0
C	+4.3 ± 1.5	CK	121.377	23.089	1993–2003	+4.2 ± 0.4	+0.1 ± 1.6
		FG	121.191	22.784	1992–2003	+12.9 ± 0.1	−8.6 ± 1.5
		LT	121.450	22.650	2001–2008	+12.7 ± 0.4	−8.4 ± 1.6
		DW	120.896	22.337	2003–2007	+6.2 ± 0.3	−1.9 ± 1.5
D	+5.0 ± 1.7	DS	121.416	25.177	1994–2008	−3.2 ± 0.2	+8.2 ± 1.7
		HC	120.912	24.850	1992–2008	+6.2 ± 1.2	−1.4 ± 2.1
		TC	120.525	24.289	2004–2008	+8.9 ± 0.5	−3.9 ± 1.7
		FY	120.283	23.900	1992–2008	+19.8 ± 0.2	−14.8 ± 1.7
		BZL	120.138	23.619	1995–2008	+57.4 ± 1.6	−52.4 ± 2.3
		JG	120.078	23.211	1992–2001	+2.9 ± 0.4	+2.1 ± 1.7
		AP	120.128	22.973	2001–2007	+16.0 ± 0.5	−11.0 ± 1.8
		PH	119.567	23.563	1998–2008	+8.6 ± 0.7	−3.6 ± 1.8
E	+1.1 ± 1.4	KS	120.281	22.619	1992–2007	+1.1 ± 0.1	+0.0 ± 1.4
		DG	120.438	22.464	2004–2008	+7.7 ± 0.4	−6.6 ± 1.4

Note: [1]ALT data series are compiled from the T/P and Jason-1 missions, from 1992 to 2008.
[2]TG rates are interseismic-phase motion free from co-seismic effects (see text for detail).

(b) Vertical motion rate determined by GPS

Station	Long. (°E)	Lat.(°N)	Start	End	Vertical rate (mm/yr)
West Profile					
GS09	121.6519	25.2086	2005/08/16	2008/12/31	−0.8 ± 0.3
TANS	121.4269	25.1815	2004/05/17	2008/12/31	−3.4 ± 0.3
KYIN	121.0804	25.04105	2004/05/22	2009/06/30	+0.4 ± 0.3
TWTF	121.1645	24.95356	2001/11/09	2009/06/30	+1.2 ± 03
HCHM	120.9846	24.7925	2006/03/17	2008/12/31	+2.0 ± 0.3
GS14	120.9595	24.8032	2005/09/13	2008/12/31	−1.0 ± 0.2
GS02	120.9823	24.8097	2004/10/30	2008/12/31	−10.6 ± 0.3
JUNA	120.8754	24.68395	2005/02/03	2008/12/31	+0.4 ± 0.2
MIAO	120.8103	24.58345	2003/05/26	2008/12/31	−5.5 ± 0.2
TASO	120.6951	24.46126	2007/11/08	2009/06/30	−4.0 ± 0.5
GS36	120.6253	24.362	2007/01/01	2009/06/30	−1.0 ± 0.3
CHIN	120.5822	24.271	2001/11/14	2009/06/30	+2.6 ± 0.3
TACH	120.5351	24.2908	2005/09/30	2009/06/30	−3.1 ± 0.2
TC12	120.5979	24.2075	2005/09/28	2009/06/30	−4.4 ± 0.2
LUKN	120.4351	24.06001	2001/11/03	2008/12/31	−3.0 ± 0.2
CHSG	120.2891	23.86034	2007/01/01	2009/06/30	−33.4 ± 0.3
JIBE	119.6133	23.74142	2006/10/02	2009/06/30	−1.9 ± 0.1
TASI	120.1888	23.72027	2007/10/31	2009/06/30	−17.8 ± 0.8
WIAN	119.4808	23.56753	2006/10/02	2009/06/30	−2.1 ± 0.1
PANG	119.5637	23.5652	1994/01/07	2005/12/26	−0.8 ± 0.2
CHYI	120.1402	23.45076	2004/02/19	2008/12/20	−33 ± 0.2
BDES	120.1719	23.38057	2007/06/12	2009/06/30	−56.6 ± 0.4
PEIM	120.1686	23.2938	2004/04/04	2009/06/30	−19.5 ± 0.4
HOKN	120.1349	23.1884	1998/11/03	2008/12/31	−12.6 ± 0.2
YSAN	120.086	23.1466	2004/12/02	2009/06/30	−6.7 ± 0.2
CKSV	120.22	22.9989	2007/01/30	2008/12/31	−3.2 ± 0.3
CKGM	120.2201	22.9988	2006/01/24	2008/12/31	+6.0 ± 0.3
GS34	120.2751	22.93922	2007/01/01	2008/12/31	−1.6 ± 0.3
ZEND	120.2176	22.9433	2006/03/29	2008/12/31	+3.4 ± 0.3
BANP	120.3054	22.6931	2007/04/03	2008/12/31	+5.2 ± 0.4
KASH	120.2883	22.6145	2004/03/09	2009/06/30	−4.3 ± 0.2
SGAN	120.3497	22.5813	2006/05/19	2009/06/30	−2.3 ± 0.3
HENC	120.7465	22.0039	1996/03/17	2008/12/31	−4.4 ± 0.3
East Profile					
LNDO	121.9181	25.0974	2003/12/05	2008/12/20	−2.9 ± 0.2
GOLI	121.9874	25.0204	2005/02/06	2008/12/20	−2.7 ± 0.2
FLON	121.9375	25.0204	2004/04/15	2008/12/20	−2.7 ± 0.3
SUAB	121.8679	24.5939	2005/06/29	2009/06/30	−5.1 ± 0.5
SUAO	121.8671	24.5924	1999/10/01	2006/10/01	−5.7 ± 0.6
NAAO	121.8102	24.4493	2004/04/06	2008/12/20	−8.9 ± 0.3
HUAP	121.7494	24.3090	2004/05/24	2009/06/30	−3.4 ± 0.4
PEPU	121.6103	24.0179	2001/11/01	2006/09/30	+0.9 ± 0.3

Table 1 (*continued*)

(b) Vertical motion rate determined by GPS

Station	Long. (°E)	Lat.(°N)	Start	End	Vertical rate (mm/yr)
East Profile					
HUAL	121.6135	23.9754	1994/01/04	2006/09/30	−6.6±0.4
HUAL*	121.6135	23.9754	1994/01/04	2008/12/20	+5.8±0.9
YENL	121.6018	23.9035	2003/01/01	2006/09/30	−12.1±0.3
SOFN	121.5982	23.8703	2005/12/10	2006/09/30	−12.6±0.3
SHUL	121.5627	23.7876	2006/07/01	2008/12/20	−15.6±0.3
JSUI	121.4239	23.4920	2003/05/13	2008/12/08	−2.7±0.4
KNKO	121.5057	23.4722	2002/04/21	2008/12/08	−3.7±0.3
NHSI	121.4530	23.4062	2005/08/13	2008/12/08	−4.7±0.3
PING	121.4543	23.3195	2002/01/22	2008/12/08	+4.5±0.3
CHEN	121.3736	23.0974	1995/01/31	2003/12/09	−1.0±0.4
CHEN*	121.3736	23.0974	1994/01/14	2008/12/31	+56.1±1.0
T101	121.3236	23.0203	2004/04/17	2008/12/08	+1.2±0.3
T102	121.2768	23.0160	2003/12/18	2008/12/08	+3.2±0.3
SINL	121.2546	22.9083	2005/06/08	2008/12/08	+3.1±0.3
S104	121.1894	22.8208	1994/03/13	2008/12/08	+2.1±0.3
FUGN	121.1922	22.7907	2003/12/10	2008/12/08	−6.7±0.3
PEIN	121.1231	22.8011	2005/08/26	2009/06/30	−9.4±0.3
LUDA	121.4759	22.6581	2003/12/15	2006/12/31	−4.0±0.3
TMAM	121.0075	22.6161	1995/03/01	2008/12/31	−5.1±0.2
DAWU	120.8900	22.3406	2005/07/27	2008/12/31	−4.1±0.3
DAJN	120.8650	22.3113	2004/06/04	2008/12/31	−4.1±0.3
LANY	121.5581	22.0373	1994/01/24	2009/06/30	+10.1±0.4
KDNM	120.7820	21.9494	1994/01/02	2009/06/30	+0.1±0.2

Note: The GPS time series are adopted from the Taiwan Earthquake research Center, for interseismic-phase motion free from co-seismic effects in recent years (mainly since 2004), except *CHEN and *HUAL, which include the 2003 Chengkung earthquake and the 2006 Hualien near-shore earthquake, respectively.

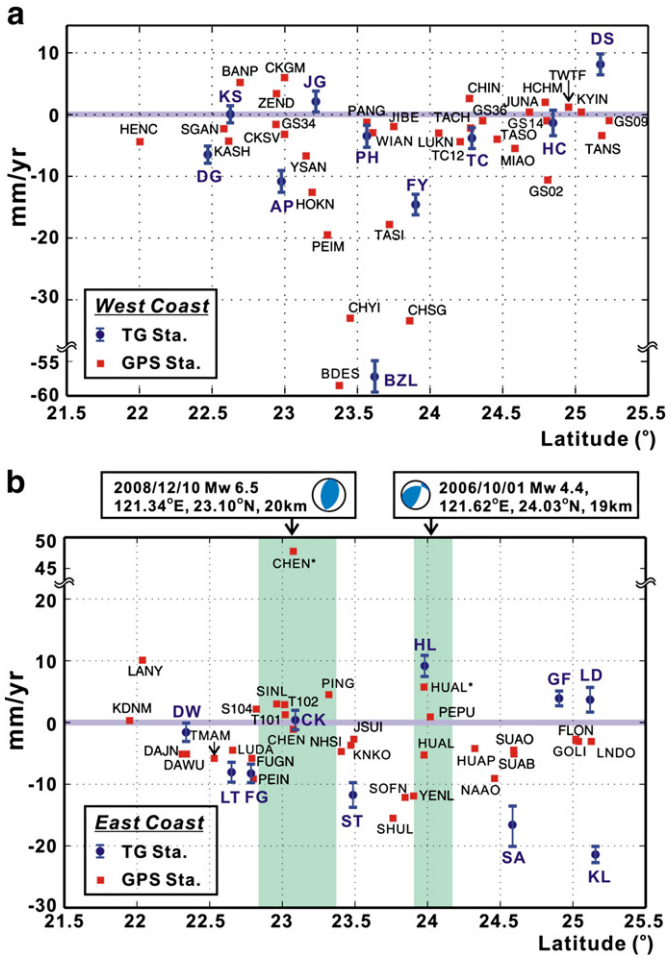

Fig. 4. Vertical crustal motion rate as functions of latitude along the two separate N–S profiles of Taiwan: (a) the west coast, and (b) the east coast. Two earthquakes (near CK and HL stations) with focal mechanism solutions are indicated in (b); their aftershock extents are highlighted in green shade.

4.1. West coast — stable tectonic basement?

On the west coast of Taiwan, the salient exception is the BZL station where occurred an extraordinary sinking as high as −52.2±2.3 mm/yr, as corroborated by the GPS results showing a large land subsidence surpassing −50 mm/yr. This is due to over-withdrawal of groundwater for aquaculture, an important economic activity in west Taiwan in the past years, according to the reports of the Groundwater Monitoring Network of the Water Resources Agency (WRA) of Taiwan (WRA official website http://www.drc.ntu.edu.tw/gwater/applications-07.php) (e.g. Fan, 2001; Liew et al., 2004). Indeed, compared with the water-level monitored by borehole instruments reporting extreme subsidence as high as 116 mm/yr during 1975–1995, our ALT–TG and the GPS measurements show a relative reduction of this anthropogenic subsidence in the recent years.

In contrast, the ALT–TG estimate of the PH station, on the western offshore islet of Penghu in the same latitude band but located off in Taiwan Strait, shows a slight subsidence at −3.6±1.8 mm/yr (Fig. 4(a), Table 1). The face values of three continuous GPS there (JIBE, PANG, and WIAN) show similar subsidence (Fig. 4(a), Table 1). Located geologically on the continental basement, the Penghu islet is presumably little influenced by the Taiwan orogeny from the east and therefore tectonically inactive (e.g. Ho, 1986). Yet there seems to be an important continental margin opening in the southeast China, of potential of petroleum reserves (e.g. Covey, 1984), while recent lithological studies stress the existence of a lateral shear zone across the Taiwan Strait in the N–S direction (Chen et al., 2006; Yokoyama et al., 2007). These observations infer that the Taiwan Strait is not tectonically inert but relates to another deformation mechanism out of the Taiwan orogeny itself.

4.2. Northern section of east coast — a complex deformation pattern

The east coast is juxtaposed next to the paralleling LV suture zone of convergence and perpendicular to the Ryukyu subduction trench at the middle. Tectonically, the Ryukyu Trench laterally collides into east Taiwan near Hualien, which is at the northern tip of the Coastal Range and LV (Fig. 1).

North of Hualien, both the ALT–TG and GPS measurements along the east coast reveal a non-uniform vertical motion in both spatial

pattern and time span, as implied in the discrepancies between the short-term GPS and the decadal ALT–TG determinations (Fig. 4, Table 1). It may be generated by local adjustment of complex deformation combining convergence with extension, an issue that can be further assured by a long-term monitoring in the northern Taiwan. It is worth noting that, barring some local effect (for example at GF) and excluding the very-short-term measurements at the LD and HL, the east ALT–TG results illustrate the northward subsidence (Fig. 4(b)). This feature can also be seen from the ground relief in eastern Taiwan. In Fig. 5a, a northward topographic dipping with a steady ~0.2° with respect to the sea level can be seen from south of Hualien (HL station) all the way to the northern offshore area of Taiwan (in a length about 170 km). This interesting inter-relationship unfortunately cannot be further verified by the relatively short spans of the GPS face values (cf. Dixon, 1991; Feigl et al., 1990), which show a clear segmented pattern well consistent with the recent co-seismic motions in a few significant earthquakes occurring in the near field along the east coast (Fig. 4b).

This northward dipping of topography may be a surface manifestation of northward subduction. Physically, an old, cold and heavy plate can drive a significant mantle flow, further inducing rapid trench rollback and regional depression. The driven convection flows can induce suction, dragging plate downward and causing the topographic subsidence near the conjunction area (Conrad and Lithgow Bertelloni, 2004).

To shed light on the possible mechanism of the slab suction in the northeast Taiwan, we shall scrutinize the thickness and age of the neighboring Philippine Sea Plate. It is common to check the elastic thickness of the oceanic lithosphere with the flexure or bending of the subducting plate, modeled as an elastic plate, at trenches bounded by the overriding plate which exerts a bending moment generated from its weight. Ultimately, the topographic feature of the forebulge at subducting plate becomes a proxy for the elastic plate thickness,

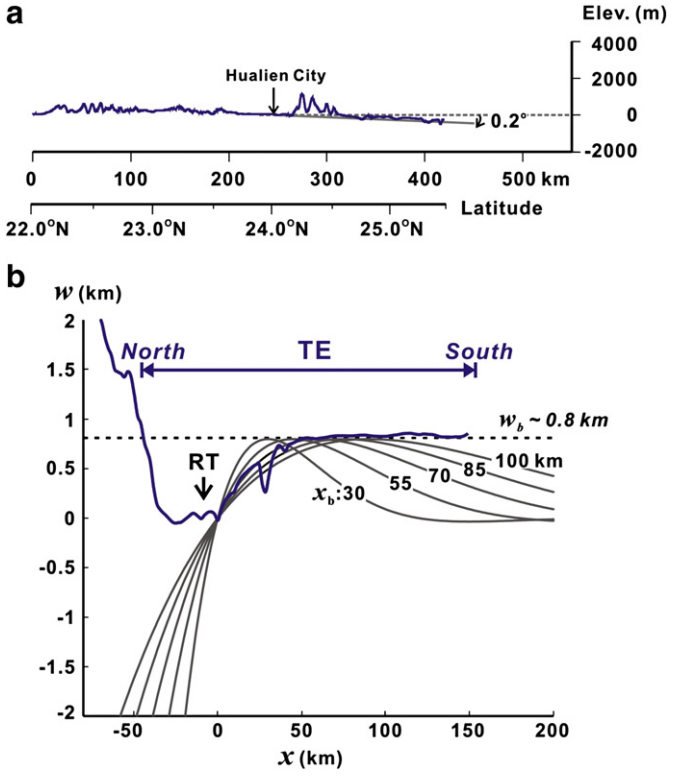

Fig. 5. (a) N–S topographic profile (T1 in Fig. 1) through the east Taiwan. (b) The flexures of oceanic lithosphere as a function of distance from forebulge (x_b), for various lithospheric elastic thicknesses. The thick curve gives the observed topographic relief along Profile TE (Fig. 1).

which is proportional to the plate's age. The height of the deflection profile of the plate ($H(x)$) can be described as (McNutt and Menard, 1982):

$$H(x) = w_b\sqrt{2}e^{\pi/4}\exp\left[\frac{-\pi}{4}\left(\frac{x-x_0}{x_b-x_0}\right)\right]\sin\left[\frac{\pi}{4}\left(\frac{x-x_0}{x_b-x_0}\right)\right] \quad (2)$$

where x and $w$are both referencing to the location where the topographic relief reaches its most bottom site along the bending plate; x_b and$w_b$respectively indicate the distance and amplitude of the forebulge accounted from the reference sitex_0. The "zero" values of the topographic relief and the distance are defined at the point where the slope of the topographic profile is "zero" along the bending oceanic plate. Fig. 5(b) demonstrates the topographic relief profile across the Ryukyu trench to the east of Taiwan (Profile TE in Fig. 1), against various synthetic lithospheric deflection profiles depending on x_b. In making the comparison, we take w_b= 0.8 km and x_b = 70 km from the DEM curves in Fig. 5(b). The elastic thickness (T_e) of the plate can then be derived (McNutt and Menard, 1982; also see Turcotte and Schubert, 2002, Equations 3–72, 3–127) to be 28–31 km, assuming the mantle density of 3300 kg/m^3, the Poisson ratio ofν = 0.25, and the Young's modulus E of the oceanic lithosphere of 70–100 GPa. The derived T_e corresponds to the age of 90 Ma or older for the western Philippine Sea plate next to Taiwan, according to the thickness–age relationship proposed by Stein and Stein (1992). Note that previously the age determination of the western Philippine Sea Plate has been uncertain, ranging from a few to one hundred million years (e.g. Deschamps et al., 2000; Richard et al., 1986; Sibuet et al., 1999). This is consistent with the assertion that the western Philippine Sea basin is an old, heavy oceanic lithosphere (Deschamps et al., 2000), which can induce a significant topographic depression adjacent to the Ryukyu Trench as required in our scenario. This appears to be a plausible mechanism for the general subsiding background observed in the northern section of Fig. 4(b).

4.3. Southern section of the east coast — a saw-tooth deformation scenario

At the northern tip of the southern section of the east coast, the city of Hualien itself is seismically active, suffering from many middle-to-large earthquakes (for example the 1951 earthquake sequence and the 2006 earthquake in this study). This leaves its "stable" TG series in short segments, hence the ALT–TG face values at the HL station may not be representative of the long-term value. Indeed, the face value determined from 1997–2002 (5 years) in Table 1 shows an apparent uplift of +8.9 ± 1.7 mm/yr. On the other hand, the nearby GPS shows an interseismic-phase subsidence at rate of about −6.6 ± 0.4 mm/yr during 1994–2006 excluding the large thrusting event of Oct. 1st, 2006, but an uplift at the rate of about +5.8 ± 0.9 mm/yr when the latter is included (indicated as HUAL* in Fig. 4(b) and Table 1). This has actual bearings on the finding of the permanent uplift left in the Hualien TG by the 1951 Hualien earthquake sequence (e.g. Ota et al., 2005). Note that this behavior is in contrast to the northward dipping trend for the other east-coast TG stations, indicating the extreme complicity of the tectonic "corner" setting of Hualien. South to the Hualien city and the Ryukyu Trench, both ALT–TG and GPS results for the vertical-motion rates quickly turn to a segmented, undulating pattern. Note that the value at LT, a small volcanic islet offshore of southeast Taiwan on the Philippine Sea plate, rides along the same trend with the other eastern stations, indicating that the vertical motion along the eastern coast of Taiwan couples with the eastern oceanic plate.

The segmented behavior of vertical crustal deformation can be recognized in the 2003 Mw 6.5 Chengkung earthquake and the recent 2006 Mw 4.4 Hualien earthquake. The green shades (Fig. 4(b)) highlight the extent of the respective coseismic slip determined by

aftershocks. The Chengkung earthquake occurred in the eastern nearshore on Dec. 10, 2003, which is apparently a reactivation of the LV fault but in a distinct segment with mainly a thrusting plus a strong lateral motion (Chen et al., 2004; Lee et al., 2006). Locations of the tide gauge station CK and the GPS station CHEN are at its hanging wall. As mentioned above, our reported ALT–TG rate value at the CK station is near zero, 0.1 ± 1.6 mm/yr, pertaining only to the interseismic phase prior to the Chengkung earthquake and excludes the influence of the earthquake. The corresponding GPS station CHEN's steady records also showed a slight subsidence at -1.0 ± 0.4 mm/yr (see Fig. 4(b)). However, taking the longer record of 1996–2008 including the coseismic thrusting of the earthquake, GPS gives an average vertical uplift motion of $+56.1 \pm 1.0$ mm/yr (indicated as CHEN* in Fig. 4(b) and Table 1), opposite in sign to the interseismic phase.

Thus, the alternating sense and amplitude of motion between the coseismic and interseismic phases can be modeled by a saw-tooth type of motion as depicted in Fig. 6. That is, slow subsidence of the region is intermittently interrupted and overtaken by a series of coseismic (plus possible short-term post-seismic) thrustings that more than reverse the interseismic subsidence trend. The net, very long-term effect then is an overall uplift of the east Taiwan (especially the coast along with the Coastal Range). The topography and geological data record the average long-term uplift shown by the envelope of the saw-tooth curve, constituting the orogeny of the Coastal Ranges of eastern Taiwan.

Considering the northward-subsiding pattern, the observed subsidence from ALT–TG and GPS in the southern section of east Taiwan (in the last decade or two) may simply be the depression of the plate with respect to the sustained subduction at the Ryukyu trench, as observed in the northern section. From this point of view, the so-called interseismic-phase motion is actually the aseismic subsidence consistent to the bending of the subducting plate. In the southern section of east Taiwan, the subduction of the Philippine Sea plate can drag down the east Taiwan (which is identified as parts of the Philippine Sea plate) and cause the regional subsidence; in the meantime the considerable thrusting in earthquakes occurs as subject to the lateral convergence of plates. Both the mechanisms of subduction and lateral collision should simultaneously affect the ground motion but in different temporal and spatial scales.

The saw-tooth behavior can accommodate the interseismic pattern in the eastern Taiwan detected by the recent leveling measurements (Chen et al., 2011), where the vertical motion exhibits a segmented pattern in the Coastal Range. This deformation model is also consistent with the geological observations in the region: the vertical motion derived from samples from Holocene coral terraces with radiocarbon and Uranium-series dating and corrected of the sea-level rise history gave uplift rates of about 5 mm/yr and 3–5 mm/yr respectively for the eastern limb of Coastal Range and the southernmost Taiwan (Peng et al., 1977; Wang and Burnett, 1990). Lacking sufficient temporal resolution that could identify any coseismic and interseismic behavior, these measurements naturally detect only the long-term uplift.

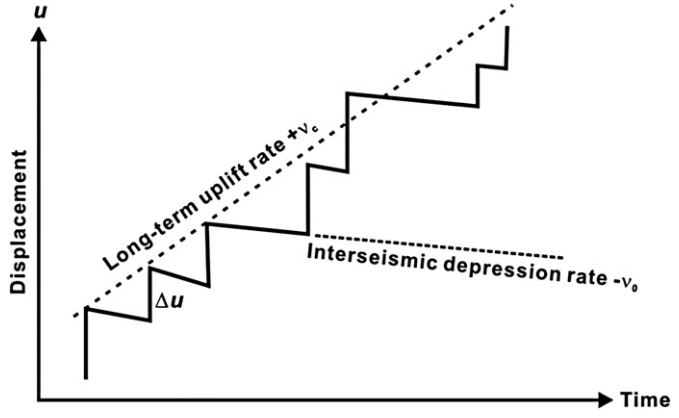

Fig. 6. Schematic model of a vertical displacement scenario for the southern segment of the east coast of Taiwan, where successive coseismic slip (Δu) and the opposite interseismic motion form a saw-tooth history for the local deformation.

On the other hand, such saw-tooth tectonic behavior is interesting in its own right in reflecting the discordance of transient-release of strain with long-term tectonic motion. Similar behavior has also been observed in other subduction areas, where the opposite motions correspond to different seismic phases, e.g. the Cascadia subduction near the junction of the southwestern Canada and northwestern USA (Dragert et al., 2001), the Sunda megathrust in West Sumatra (Sieh et al., 2008). All these cases elucidate on the deformation process in subduction seismogenic zone, and further reveal the fact that the subducting plate would play a decisive role in the convergence not only affecting local or regional topography but also the earthquake cycle.

5. Conclusions

Using the decadal ALT–TG measurements and the more recent GPS data, we obtain a comprehensive determination of vertical motion around the coast of the island of Taiwan controlled by an active tectonic convergent complex. We find the following:

(1) We confirm for the first time the general pattern of subsidence of the entire Taiwan coast during our studied period of the past 1–2 decades. From the values in Table 1 (and Figs. 2 and 4), we see that overall the TG rates are mostly strongly positive while the ALT rates are also positive but significantly smaller (although at 4–5 mm/yr the latter is still twice the global average.) The net result then is a general negative ALT–TG, giving the overall pattern of subsidence along most of the Taiwan coast. The vertical motion rates from the ALT–TG and GPS measurements can be represented with a rough (unweighted) mean value of about −4.5 mm/yr and −2.6 mm/yr, respectively (excluding the measurements around the BZL station).

(2) The west coast sees no prominent vertical motion, with only a small overall subsidence of land, suggesting weak orogenic buckling consistent with a foreland basin away from the active orogeny along with sediment compactions. The only exception is an extraordinary local subsidence seen in the middle section, which is known for years to be a consequence of the over-withdrawal of groundwater for aquaculture. Our ALT–TG and the GPS measurements show a slight reduction of this anthropogenic subsidence in the most recent years.

(3) Both the ALT–TG and GPS estimates of the Penghu islet show a slight subsidence. This suggests that the Taiwan Strait is not tectonically inert but relates to some distinct deformation mechanism out of the Taiwan orogeny.

(4) The different regimes of tectonic influence along the east coast manifest themselves in the complex behavior in their vertical crustal motion. In the northern section, we raise the mechanism of mantle flow suction for the regional subsidence response. The plate flexure indicates that the adjacent Philippine Sea plate is an old, thick oceanic plate, which can drive slab dragging in the east Taiwan, manifesting in a gentle northward down-dip of the topography along this section. In the southern section of the east coast, judging from the different behavior between the coseismic and interseismic vertical motions marked by the major earthquakes during the studied period, we postulate a temporal saw-tooth scenario for the deformation in different phases. It demonstrates the opposite motions affected by the different mechanisms in the frontal sections of the subduction zone. These different motions can be understood with lateral collision and slab dragging subject to varied temporal and spatial dependence.

Acknowledgments

We thank the Central Weather Bureau of Taiwan for the tide gauge data, and the Taiwan Earthquake research Center (TEC) and the Academia Sinica for the GPS data (courtesy of Drs. Suei-Bei Yu and Long-Chen Kuo). Assistance from Dr. Chung-Yen Kuo on altimeter data processing is also acknowledged. The reviewers helped greatly in improving the manuscript. This study is supported by the National Science Council of Taiwan, under Grants NSC 97-2745-M-002-012, 100-3113-M-002-002, and 100-2611-M-002-008.

References

Angelier, J., Chang, E.T.Y., Hu, J.C., Chang, C.P., Siame, L., Lee, J.C., Deffontaines, B., Chu, H.T., Lu, C.Y., 2009. Does extrusion occurs at both tips of the Taiwan collision belt? Insights from active deformation studies in the Ilan Plain and Pingtung Plain regions. Tectonophysics 466, 356–376.

Cazenave, A., Nerem, R.S., 2004. Present-day sea level change: observations and causes. Reviews of Geophysics 42, RG3001. doi:10.1029/2003RG000139.

Cazenave, A.K. Dominh, Ponchaut, F., Soudarin, L., Cretaux, J.F., Le Provost, C., 1999. Sea level changes from Topex–Poseidon altimetry and tide gauges, and vertical crustal motions from DORIS. Geophysical Research Letters 26, 2077–2080.

Chang, C.P., Chang, E.T.Y., Angelier, J., Kao, H., Lee, J.C., Yu, S.B., 2003. Stress and strain field in Taiwan oblique convergent system: constrains from GPS observations and tectonic data. Earth and Planetary Science Letters 214, 115–127.

Chang, C.P., Chen, K.S., Wang, C.T., Yen, J.Y., Chang, T.Y., Lin, C.W., 2004. Application of space-borne radar interferometry on crustal deformations in Taiwan; a perspective from the nature of events. TAO 15 (3), 523–543.

Chen, H.Y., Yu, S.B., Kuo, L.C., Liu, C.C., 2004. Coseimic and postseismic displacements of the 10 December 2003, Mw 6.5 Chengkung eastern Taiwan, earthquake. The 2004 International Symposium on GNSS/GPS, Dec. 6th -8th, Sydney, Australia.

Chen, C.H., Lu, H.Y., Lin, W., Lee, C.Y., 2006. Thermal event records in SE China coastal areas: constraints from Monazite ages of beach sands from two sides of the Taiwan Strait. Chemical Geology 231, 118–134.

Chen, K.-H., Yang, M., Huang, Y.-T., Ching, K.-E., Rau, R.-J., 2011. Vertical displacement rate field of Taiwan from geodetic leveling data 2000–2008. Survey Review 43 (321), 296–302.

Chiu, Y.T., Ching, K.E., Hou, C.S., Hu, J.C., Rau, R.J., 2008. Crustal deformation of Ilan plain from GPS observations, 2002–2006. Central Geological Survey Special Publication 20, 111–124.

Church, J.A., White, N.J., Coleman, R., Lambeck, K., Mitrovica, J., 2004. Estimates of the regional distribution of sea level rise over the 1950–2000 period. Journal of Climate 17, 2609–2625.

Conrad, C.P., Lithgow Bertelloni, C., 2004. The temporal evolution of plate driving forces: importance of "slab suction" versus "slab pull" during the Cenozoic. Journal of Geophysical Research 109, B10407. doi:10.1029/2004JB002991.

Covey, M., 1984. Lithofacies analysis and basin reconstruction, Plio-Pleistocene western Taiwan foredeep. Petroleum Geology of Taiwan 20, 53–83.

Dadson, S.J., Hovius, N., Chen, H., Bade, W., Hsieh, M.L., Willet, S., Hu, J.C., Horng, M.J., Chen, M.C., Stark, C.P., Lague, D., Lin, J.C., 2003. Links between erosion, runoff variability and seismicity in the Taiwan orogen. Nature 426, 648–651.

Deschamps, A., Monié, P., Lallemand, S., Hsu, S.K., Yeh, K.Y., 2000. Evidence for early Cretaceous oceanic crust trapped in the Philippine Sea plate. Earth and Planetary Science Letters 179, 503–516.

Dixon, T.H., 1991. An introduction to the Global Positional System and some geological applications. Reviews of Geophysics 29, 249–276.

Dragert, H., Wang, K., James, T.S., 2001. A silent slip event on the deeper Cascadia subduction interface. Science 292, 1525–1528.

Ernst, W.G., 1977. Olistostromes and included ophiolite debris from the Coastal Range of eastern Taiwan. Memoirs: Geological Society of China 2, 97–114.

Fan, K.L., 2001. Some coastal environmental problems in Taiwan. Acta Oceanographica Taiwanica 39, 1–10.

Feigl, K.L., King, E.W., Jordan, T.H., 1990. Geodetic measurement of tectonic deformation in Santa Maria fold and thrust belt, California. Journal of Geophysical Research 95 (B3), 2679–2699.

García, D., Vigo, I., Chao, B.F., Martínez, M.C., 2007. Vertical crustal motion along the Mediterranean and Black Sea coast derived from ocean altimetry and tide gauge data. Pure and Applied Geophysics 164, 851–853.

Hager, B.H., King, R.W., Murray, M.H., 1991. Measurement of crustal deformation using the Global Positioning System. Annual Review of Earth and Planetary Sciences 19, 351–382.

Ho, C.S., 1986. A synthesis of the geologic evolution of Taiwan. Tectonophysics 125, 1–16.

Hsu, T.L., 1956. Geology of the coastal range, eastern Taiwan. Bulletin. Geological Survey, Taiwan 8, 39–63.

Hugentobler, U., Schar, S., Fridez, P., Beutler, E., 2001. Bernese GPS Software: Version 4.2, Astronomical Institute. Astronomical Institute, University of Bern.

Hwang, C., Guo, J., Deng, X., Hsu, H.Y., Liu, Y., 2006. Coastal gravity anomaly from retracked Geosat/GM altimetry: improvement, limitation and the role of airborne gravity data. Journal of Geodesy. doi:10.1007/s00190-062-0052-x.

Kuo, L.C., 2008. The auto-processing system for Taiwan GPS and earth science researches, The technique Report of the Institute of Earth Sciences, Academia Sinica, Origin in Chinese.

Kuo, C.Y., Shum, C.K., Braun, A., Mitrovica, J.X., 2004. Vertical crustal motion determined by satellite altimetry and tide gauge data in Fennoscandia. Geophysical Research Letters 31, L01608. doi:10.1029/2003GL019106.

Lee, J.C., Chu, H.C., Angelier, J., Hu, J.C., Chen, H.Y., Yu, S.B., 2006. Quantitative analysis of surface coseismic faulting and postseismic creep accompanying the 2003, Mw = 6.5, Chengkung earthquake in eastern Taiwan. Journal of Geophysical Research 111. doi:10.1029/2005JB003612.

Liew, P.M., Hsieh, M.L., Shyu, B.H., 2004. An overview of coastal development in a young mountain belt—Taiwan. Quaternary International 115–116, 39–45.

Luthcke, S.B., Zelensky, N.P., Rowlands, D.D., Lemoine, F.G., Williams, T.A., 2003. The 1-centimeter orbit: Jason-1 precision orbit determination using GPS, SLR, DORIS, and altimetry data. Marine Geodesy 26, 399–421.

Mazzotti, S., Jones, C., Thomson, R.E., 2008. Relative and absolute sea level rise in western Canada and northwestern United States from a combined tide gauge–GPS analysis. Journal of Geophysical Research 113, C11019. doi:10.1029/2008JC004835.

McNutt, M.K., Menard, H.W., 1982. Constraints on yield strength in the oceanic lithosphere derived from observations of flexure. Geophysical Journal of the Royal Astronomical Society 71, 363–394.

Naeije, M., Doornbos, E., Mathers, L., Scharroo, R., Schrama, E., Visser, P., 2002. Radar altimeter database system: exploitation and extension, RADSxx. Final Report. SRON/NIVR/DEOS publ., NUSP-2 report 02–06, NUSP-2 project 6.3/IS-66. ISBN: 90-5623-077-8.

Nerem, R.S., Mitchum, G.T., 2002. Estimates of vertical crustal motion derived from differences of TOPEX/Poseidon and tide gauge sea level measurements. Geophysical Research Letters 29, 1934. doi:10.1029/2002GL015037.

Ota, Y., Chen, Y.G., Chen, W.S., 2005. Review of paleoseismological and active fault studies in Taiwan in the light of the Chichi earthquake of September 21, 1999. Tectonophysics 408, 63–77.

Peng, T.H., Li, Y.H., Li, F.T., 1977. Tectonic uplift rates for the Taiwan island since the early Holocene. Memoirs: Geological Society of China 2, 57–69.

Rau, R.J., Ching, K.E., Hu, J.C., Lee, J.C., 2008. Crustal deformation and block kinematics in transition from collision to subduction: GPS measurements in northern Taiwan. Journal of Geophysical Research 1995–2005. doi:10.1029/2007JB005414.

Richard, M.A., Bellon, H., Maury, R.C., Barrier, E., Juang, W.S., 1986. Miocene to recent volcanism in eastern Taiwan K–Ar ages and petrography. Tectonophysics 125, 87–102.

Schrama, E., Scharroo, R., Naeije, M., 2000. Radar altimeter database system, RADS: towards a generic multi-satellite altimeter database system. final report, 88, SRON/BCRS publ., USP-2 report 00–11.

Sibuet, J.C., Hsu, S.K., Le Pichon, X., Le Formal, J.P., Reed, D., Moore, G., Liu, C.S., 1999. Philippine Sea Plate and Taiwan Sea Plate: formation of Taiwan. Abstract in SEASI Conference, 21, May 9–12th, Montpellier, France.

Sieh, K., Natawidjaja, D.H., Meltzner, A.J., Shen, C.C., Cheng, H., Li, K.S., Suwargadi, B.W., Galetzka, J., Philibosian, B., Edwards, R.L., 2008. Earthquake supercycles inferred from sea-level changes recorded in the corals of west Sumatra. Science 322, 1674–1678.

Stein, C.A., Stein, S., 1992. A model for the global variation in oceanic depth and heat flow with lithospheric age. Nature 359, 123–129.

Taylor, J.R., 1997. Chapter 8: Least-squares fitting. An introduction to error analysis. University Science Books (181–193).

Teng, L.S., 1996. Extensional collapse of the northern Taiwan mountain belt. Geology 24 (10), 949–952.

Tsai, Y.B., 1986. Seismotectonics of Taiwan. Tectonophysics 125, 17–37.

Tseng, Y.H., Breaker, L.C., Chang, E.T.Y., 2009. Sea level variations in the regional seas around Taiwan. Journal of the Oceanography 66, 27–39.

Turcotte, D.L., Schubert, G., 2002. Geodynamics, 2nd ed. Cambridge University Press, Cambridge, New York, Melbourne (456).

Vignudelli, S., Cipollini, P., Roblou, L., Lyard, F., Gasparini, G.P., Manzella, G.M.R., Astraldi, M., 2005. Improved satellite altimetry in coastal systems: case study of the Corsica Channel, Mediterranean Sea. Geophysical Research Letters 32, L07608. doi:10.1029/2005GL22602.

Wang, C.H., Burnett, W.C., 1990. Holocene mean uplift rates across an active plate-collision boundary in Taiwan. Science 248, 204–206.

Wu, F.T., Liang, W.T., Lee, J.C., Benz, H., 2009. A model for the termination of the Ryukyu subduction zone against Taiwan: a junction of collision, subduction/separation, and subduction boundaries. Journal of Geophysical Research 114. doi:10.1029/2008JB005950.

Yokoyama, K., Tsutsumi, Y., Lee, C.S., Shen, J.J.S., Lan, C.Y., Zhao, L., 2007. Provenance study of tertiary sandstones from the Western foothills and Hsuehshan Range, Taiwan. Bulletin of the National Museum Natural Science, Series C 33, 7–26.

Yu, S.B., Kuo, L.C., 2001. Present-day crustal motion along the Longitudinal Valley fault, eastern Taiwan. Tectonophysics 333, 199–217.

Yu, S.B., Chen, H.Y., Kuo, L.C., 1997. Velocity field of GPS stations in the Taiwan area. Tectonophysics 274, 41–59.